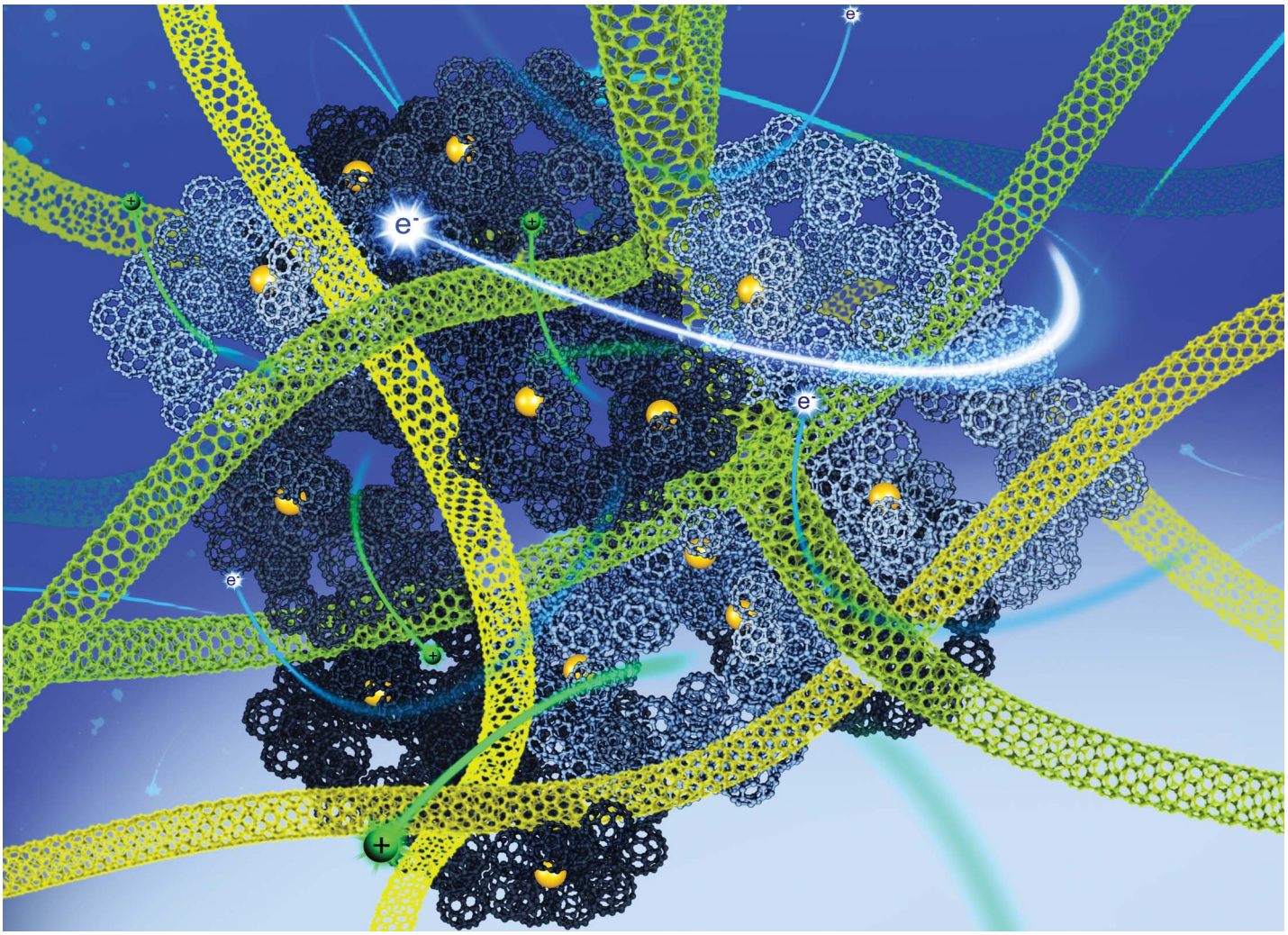

Showcasing the work of flexible all-carbon nanoarchitectures for lithium-sulfur batteries presented by Prof. Qiang Zhang, Department of Chemical Engineering, Tsinghua University.

Title: Flexible all-carbon interlinked nanoarchitectures as cathode scaffolds for high-rate lithium–sulfur batteries

A rational design of sulfur cathode based on the interlinked all-carbon scaffolds was proposed for high-rate lithium–sulfur batteries. Long carbon nanotubes were employed to form highly efficient conductive networks and graphene-based carbon nanocages welded in the scaffolds served as the building blocks for sulfur accommodation. This flexible all-carbon nanoarchitecture has superior specific capacity and extraordinary rate performance.

As featured in:

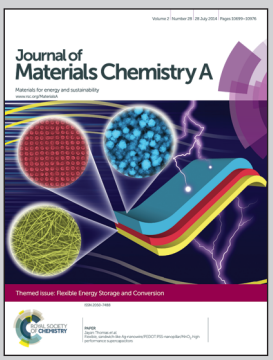

See Qiang Zhang *et al.*, *J. Mater. Chem. A*, 2014, **2**, 10869.

ROYAL SOCIETY OF CHEMISTRY

www.rsc.org/MaterialsA

Registered charity number: 207890

Journal of Materials Chemistry A

PAPER

View Article Online
View Journal | View Issue

Cite this: J. Mater. Chem. A, 2014, 2, 10869

Flexible all-carbon interlinked nanoarchitectures as cathode scaffolds for high-rate lithium–sulfur batteries†

Jia-Qi Huang, Hong-Jie Peng, Xin-Yan Liu, Jing-Qi Nie, Xin-Bing Cheng, Qiang Zhang* and Fei Wei

Received 15th January 2014
Accepted 29th January 2014

DOI: 10.1039/c4ta00245h

www.rsc.org/MaterialsA

With the development of flexible electronics, great attention has been drawn by flexible batteries as a promising power source in the emerging field of flexible and wearable electronic devices. Considering the limitation of lithium ion batteries in energy density, lithium–sulfur batteries hold the promise to be the next generation of high energy density battery systems. Despite the great efforts devoted to exploring the cathode building block units based on nanocarbon materials, the rational design of the flexible cathode scaffold is still a challenge. Herein, we demonstrated the rational design of a sulfur cathode based on interlinked all-carbon scaffolds. Long carbon nanotubes (CNTs) were employed to form highly efficient conductive networks and MgO-templated carbon nanocages were used as building blocks for sulfur accommodation. The graphene-based carbon nanocages were directly generated and welded in the CNT networks. Electrochemical evaluation indicates that the rationally-designed structure endows the sulfur cathode with a high specific capacity and rate performance. The initial discharge capacity of the electrode reaches up to 1354 mAh g^{-1} at 0.34 A g^{-1}. Even at a current density of 8.35 A g^{-1}, a reversible capacity of 750 mAh g^{-1} can still be preserved, which is 70% of that at 0.84 A g^{-1}. Such a versatile method for the construction of electrode scaffolds shows potential for flexible electrodes in high performance lithium ion batteries and supercapacitors.

1. Introduction

Battery technology has been significantly driven by portable devices, especially flexible electronics, which have been demonstrated for a wide range of applications including digital memory, rolled-up displays, implantable devices, touch screens, conformable active radio-frequency identification tags, wearable sensors, and so on.[1–4] It is predicted that the market of flexible electronics will grow both rapidly and continuously.[2,3,5] In the past few years, flexible lithium ion batteries have attracted great interest as the candidate battery system in flexible electronics,[1] and while the intrinsic electrochemical characteristics based on intercalation chemistry limit the fabrication of high energy density flexible batteries an alternative high-energy system is highly demanded. The lithium–sulfur system has a high theoretical energy density of 2600 W·h kg^{-1}, which is 3–5 times that of the theoretical value for lithium ion batteries.[6] The energy density of the lithium–sulfur battery is expected to reach over 500 W·h kg^{-1} in the future, and the abundant resources of sulfur and facile procedures for cathode fabrication bring lithium–sulfur cells towards practical applications in flexible electronics.

However, the lithium–sulfur system still faces several main obstacles due to its electrochemical nature, such as the insulating nature of sulfur and Li_2S, the relatively low density of active materials, the volume fluctuation during cycling, and the shuttle mechanism caused by the dissolution and diffusion of reaction intermediates. These hindrances cause the relatively low sulfur loading amount of the cathode materials, and the low cycling stability, limiting the overall performance. Up till now, main concerns have been paid on the cathode side of lithium–sulfur batteries, and nanocomposites have been widely used as the sulfur cathode to solve the problems in the conductivity and the volume changes of the electrodes.[7] Different building blocks including porous carbon,[8,9] carbon fiber cloth,[10] carbon nanotubes (CNTs),[11–13] carbon spheres,[14] carbide-derived carbon,[15] and graphene,[16,17] have been applied as the scaffolds for sulfur materials. The introduction of nanocarbon into sulfur cathodes showed a remarkable improvement in the electrochemical performance. Nevertheless, further improvement beyond the scale of the building block is still very much required, which calls for the rational design of hierarchical nanostructures of the flexible electrode scaffolds.

Beijing Key Laboratory of Green Chemical Reaction Engineering and Technology, Department of Chemical Engineering, Tsinghua University, Beijing 100084, China. E-mail: zhang-qiang@mails.tsinghua.edu.cn

† Electronic supplementary information (ESI) available: SEM image of the dispersed long CNTs, TEM image and the pore distribution of the carbon nanocages. See DOI: 10.1039/c4ta00245h

For the development of flexible electrodes, one of the major challenges is to achieve a mechanically robust, lightweight system without compromising the electrochemical characteristics. This also requires innovation on the structural design of the flexible electrode and the choice of the scaffold materials. Benefiting from their high chemical stability and electrical conductivity, carbon nanomaterials have been widely applied in electrochemical applications.[18] For instance, one-dimensional CNTs possess outstanding performance when serving as conducting additives or electrode materials themselves because of their high efficiency in forming conducting networks in electrodes.[3,19] Wrinkled graphene materials are also candidates as building blocks for lithium–sulfur batteries due to their highly conducting nature and their ability to accommodate active materials.[11,17,20] The rational design of the three-dimensional (3D) electrode based on the intrinsic properties of different building blocks offers even better electrode materials for superior batteries with a high energy density and good stability.[7,21–24] For instance, Kaskel's group reported mechanically stable and highly flexible freestanding multi-walled CNT/DUT-19 carbide-derived carbon/sulfur composite cathode foils with tunable sulfur loading, high in-plane conductivity, and enhanced cycling stability;[25] Wang, Abruña, and co-workers proposed novel hierarchical architecture multi-walled CNT@meso C core–shell nanostructures as a carbon matrix for the effective trapping of sulfur/polysulfides as a cathode material for lithium–sulfur batteries;[22] Wang's group explored micro-sized spherical porous carbon/CNT/sulfur composites with a high tap density and high sulfur content to decrease the resistance of the composite, and allow for improved high-current-density performance for lithium–sulfur batteries;[23] we reported the hybrids of graphene and single-walled CNTs[26] as well as graphene/CNT/porous carbon as 3D conductive scaffolds for high-rate lithium–sulfur batteries. Generally, the combination of different building blocks is commonly realized by direct mechanical mixing. Although this is the most facile method to achieve the composite materials, the interfaces between building blocks are weak; therefore, both the mechanical strength and the electrical conductivity of the composite electrodes are not satisfying. Other methods have been employed to introduce weak chemistry such as hydrogen bonds or electrostatic interaction to assist the formation of composite materials,[27] which similarly limit the full utilization of the conductivity of the building blocks. According to the demand for a high-performance sulfur cathode towards flexible lithium–sulfur batteries, carbon scaffolds are required with following characteristics: (1) high electrical conductivity throughout the whole of the cathode scaffold; (2) high accommodation capability for the sulfur active materials; and (3) high mechanical strength to withstand the volume change during repeated charge/discharge process. The rational design of the flexible cathode materials for high-performance lithium–sulfur batteries is still in high demand.

In this contribution, we explore the idea to fabricate flexible electrodes with rational pore structures and conducting networks by the incorporation of CNTs and mesoporous graphene-based materials. These two such building blocks are integrated through carbon deposition *via* high-temperature chemical vapour deposition (CVD), which ensures the high electrical conductivity throughout the whole electrode as well as the extraordinary mechanical stability. In the as-obtained all-carbon flexible cathode scaffold, long CNTs are intercrossed in the whole cathode and interlinked with other building blocks to form the highly efficient 3D conductive network as a rapidly long-range electron highway. The graphene-based carbon nanocages derived from MgO templates were with high intrinsic electrical conductivity and sufficient meso-scale space to accommodate sulfur, which is expected to restrain the polysulfide shuttle. Such a binder-free binary-CNT/graphene-based flexible nanoarchitecture demonstrates the capability for high-rate lithium–sulfur batteries, avoiding the undesirable blockage of electron pathways by insulative polymeric binders and electrochemical corrosion of metal current collectors. The high sulfur loading amount of 2.3 mg cm^{-2} can be achieved by incorporating sulfur into the 3D scaffold, which is much higher than the sulfur loading on conventional electrodes with metal foil current collectors through the slurry strategy. Moreover, the flexibility of such 3D cathodes will also meet the increasing demands for flexible electronic devices.

2. Results and discussion

To realize the rational design of the flexible scaffolds for sulfur cathodes, an efficient electronic pathway, a robust mechanical structural network, together with a building block with high sulfur accommodation are absolutely required. Two typical nanostructures were employed to demonstrate this rational design concept, namely, ultra-long CNTs were applied to form a highly conductive network and contribute to the structural strength, and a MgO-templated mesoporous graphene-based carbon nanocage with ultra-high surface area, few-layered graphene walls, and mesopore volume serves as a bifunctional building block to accommodate active sulfur materials and afford superior short-range conductivity. The morphologies of the two building blocks were illustrated as Fig. S1a and S1b.† On one hand, the ultra-long CNTs applied herein were dispersed from 2.0 mm-long vertically aligned CNTs. They were had a length of 300–700 μm after dispersion. Such ultra-long CNTs can be interlinked into a 3D network with both robust mechanical strength and high electronic conductivity.[3] On the other hand, carbon nanocages grown on MgO nanoparticles through the high-temperature CVD of methane contained abundant mesopores, and the walls of the nanocages are composed of few-layered graphene. As indicated by the N_2 isothermal adsorption/desorption test, the carbon nanocages exhibited an ultrahigh pore volume of 5.5 mL g^{-1} originating from mesopores at 5–10 nm. Such 3D building blocks with a high surface area and interconnected mesopores are in favour of sulfur storage with extraordinary contact as composite cathode materials.

In order to rationally integrate the building blocks of CNTs and carbon nanocages, an *in situ* CVD strategy was applied to form highly-conductive and highly-interlinked conductive 3D networks. As shown in Fig. 1, the MgO nanoflakes were

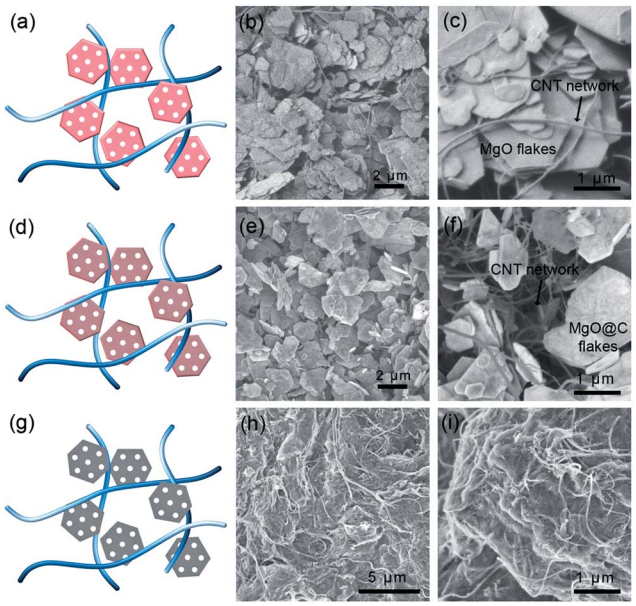

Fig. 1 The fabrication of all-carbon flexible film through an *in situ* facile template strategy: (a) schematic of CNT/MgO composite; (b) and (c) SEM images of CNT/MgO composite; (d) schematic of CNT/carbon nanocage deposited on the MgO (MgO@C) composite; (e) and (f) SEM images of the CNT/MgO@C composite; (g) schematic of CNT/carbon nanocage composite; (h) and (i) SEM images of CNT/carbon nanocage composite.

uniformly distributed among the flexible CNT network through a filtration method. The graphene-based nanocages were removed by facile acid leaching. As indicated in Fig. 1a–c, the ultra-long CNTs were intercrossed among the MgO nanoflakes. Benefiting from the ultrahigh aspect ratio of the ultra-long CNTs, they served as a skeleton and afforded the CNTs/MgO composite as a free-standing flexible film when the CNT content was as low as 5 wt%. Such a structure was similar to the flexible CNT/activated carbon film of supercapacitors.[28] Herein the hexagon-like MgO flakes had a diameter of 1–5 μm and a thickness of less than 80 nm. The areal densities of the CNTs and MgO in the freestanding film were 0.53 and 16.0 mg cm^{-2}, respectively. The free-standing film was then subjected to 950 °C high-temperature CVD with methane as the carbon source to obtain the CNT/MgO@C hybrid structure. During nanocarbon deposition, the methane was dehydrogenated on the surface of the MgO template to form the 3D nanocage, which is also welded to the long CNT network to form an interconnected and robust 3D scaffold (Fig. 1d–f and 2). Such intercrossed nanostructures were well preserved even after the removal of the MgO templates (Fig. 1g–i), and the as-derived all-carbon film was free-standing and flexible.

According to the Raman spectra (Fig. 3a), the CNT/MgO composites present typical spectra of CNTs with a low I_D/I_G ratio of 0.42. The CNT/MgO@C composite possessed a larger I_D/I_G ratio of 0.96, which was attributed to the deposition of carbon nanocages with a smaller graphene domain size and more edges. After the facile removal of the MgO template using dilute hydrochloric acid, an all-carbon interlinked nanoarchitecture

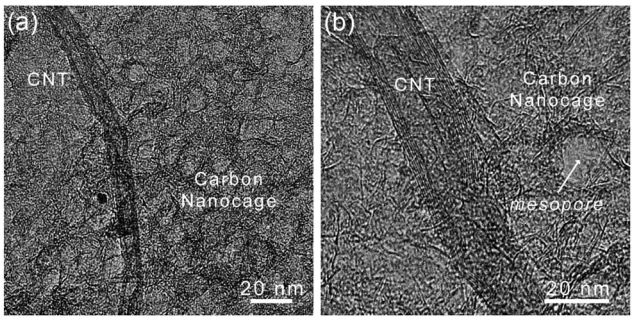

Fig. 2 (a) TEM image of the CNT/carbon nanocage composite; (b) high-resolution TEM image showing the welded CNT and carbon nanocage composite.

for a flexible cathode scaffold can be available. The interlinked networks were well preserved (Fig. 1h). The nanocage replicated the hexagonal structure of the MgO template and the subtle structure exhibited a sponge/foam-like morphology, which was in good accordance with the highly mesoporous nature (Fig. 1i). The TEM images (Fig. 2a and 2b) of the composite showed that the CNTs were in good contact with the carbon nanocage flakes. There were mainly 5–10 nm mesopores in the carbon nanocages. To confirm whether the *in situ* CVD realized welding of the CNTs and carbon nanocages together and enhanced the electrical conductivity, the conductivities of CNT/carbon nanocage composite film fabricated by *in situ* CVD or direct mixing/filtration were compared. The conductivities measured by four-probe method indicated that the CNT/carbon nanocage flexible scaffold fabricated by *in situ* CVD exhibited a conductivity of 62.9 S cm^{-1}, much higher than 18.7 S cm^{-1} for the one obtained by mechanical mixing. The three-fold improvement was attributed to the carbon deposition during CVD, which linked long-range conducting CNTs and the carbon nanocage building blocks.

Thermal gravimetric analysis (TGA) was conducted to determine the mass ratio of carbon nanocage to the CNT network in the flexible scaffold. As shown in Fig. 3b, the thermal gravimetric (TG) profile indicated a two-step weight loss behaviour. These two weight loss periods were assigned to the oxidation of carbon nanocages with lower thermal stability (peak at 545 °C) and the oxidation of CNTs with higher thermal stability (peak at 621 °C). Consequently, the areal densities of

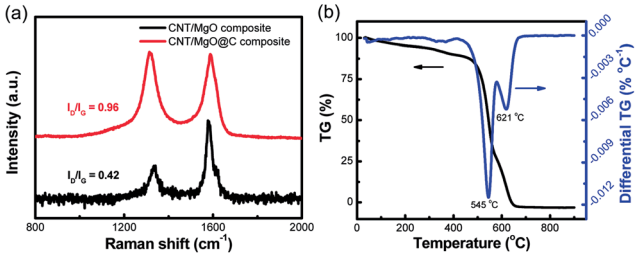

Fig. 3 (a) Raman spectra of the CNT/MgO composite and CNT/MgO@C composite; (b) the TG and differential TG curves of the CNT/carbon nanocage composite.

the CNTs and carbon nanocages were determined to be 0.52 and 1.04 mg cm^{-2}, respectively.

Towards applications in flexible energy storage devices, the mechanical property of the flexible electrodes is of great importance. As shown in Fig. 4a, at low strain (I), the interaction between CNTs and nanocages was limited due to the loose packing of the building blocks in the flexible membrane; as deformation increased, the soft CNTs stretched to accommodate the deformation (II); therefore, the CNT/nanocage nanocomposites turned stiffer, which improved the load-bearing capability in the axial direction. Based on good interfacial bonding with the CNTs, the nanocomposite strength improved with increasing deformation. Such a phenomenon was pronounced for ultra-long CNTs, which provided a large number of anchoring sites for stress transfer.[29] High deformation was also detected (Fig. 4a). Thus, at high deformation (III), the CNTs were highly stretched and aligned along the stretching direction. In order to further confirm the reinforcement mechanism, the structure and morphology of the all-carbon composites after stretching were characterized by electron microscopy. The SEM image shown in Fig. 4b displays that the entire cross-sections of the long-CNT-reinforced nanocomposites were rough, and many ruptured CNTs rather than pulled out CNTs were visually presented on the fracture edges. This is a clear evidence of the strong interfacial adhesion between the CNTs and carbon nanocages. The CNT/carbon nanocage film has a tensile strength of 2.75 MPa and an elongation-at-break of 7.30%. Active sulfur materials showed a volume change of over 70% in the lithiated and delithiated states. The elastic property of the all-carbon scaffold may sustain this huge volume change during charge/discharge cycles and benefits the overall electrochemical performance of this cathode.

After the sulfur incorporation through heat infiltration, a free-standing sulfur film cathode was obtained (Fig. 5). The morphology of the film was well preserved during sulfur incorporation, and the thickness of the film was determined to be *ca.* 50 μm. The sulfur content in the electrode reached 60 wt% with an areal density of 2.3 mg cm^{-2}, which was much higher than the routine doctor blade method.[9,13,26,30,31] Despite the high-areal sulfur loading, the all-carbon interlinked structure ensured the mechanical strength of the sulfur-containing film, which was still bendable (Fig. 5d). Although the thickness

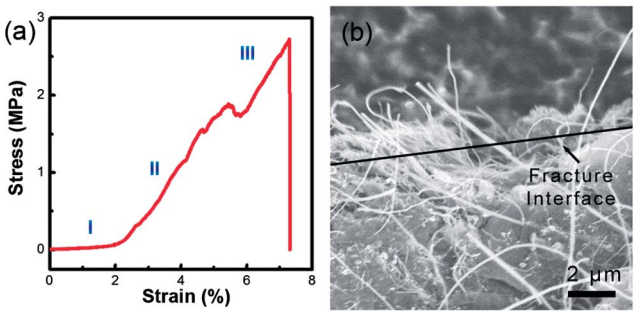

Fig. 4 (a) The typical stress–strain curves of CNT/carbon nanocage composite film; (b) SEM image of the fracture interface for CNT/carbon nanocage composite.

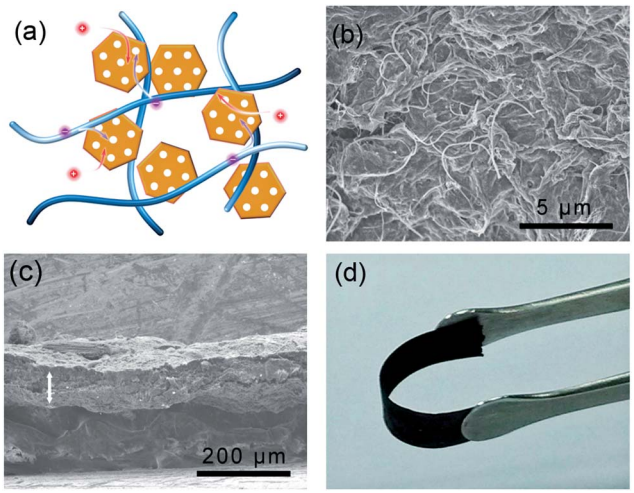

Fig. 5 (a) Schematic of sulfur cathode with CNT/carbon nanocage as scaffold; (b) SEM image of sulfur/CNT/carbon nanocage composite; (c) side view SEM image of the flexible sulfur/CNT/carbon nanocage electrode; (d) optical image of the flexible sulfur cathode membrane.

of the as-obtained electrode film reached 50 μm, it was expected that superior electrochemical performance was available on the rationally designed nanostructures with CNTs as highly efficient conducting networks and carbon nanocages as bifunctional sulfur reservoirs.

Cyclic voltammetry (CV) was employed to investigate the electrochemical behaviour (Fig. 6a). The cathodic scan presented a typical two-step reduction of sulfur to high-order polysulfide and Li_2S/Li_2S_2, respectively. While in the anodic scan, the oxidation peak at 2.36 V corresponded to the transformation of sulfides to high-order polysulfides, and eventually to elemental sulfur.[26,31] The profiles overlapped well within the CV cycles, suggesting a good electrochemical reversibility of the flexible electrodes. Fig. 6b describes the galvanostatic cycling performance of the sulfur electrode, including 4 cycles at 0.34 A g^{-1} and subsequently 50 cycles at 1.67 A g^{-1}. The initial discharge capacity of the electrode reached up to 1354 mAh g^{-1}. With an elevated current density of 1.67 A g^{-1}, the discharge capacity decreased to 953 mAh g^{-1} while maintaining well at 892 mAh g^{-1} after 50 cycles. Owing to the interconnected porous nanostructures and hybrid short-/long-range conductive scaffolds, the flexible cathodes also exhibited outstanding high rate capability. The rate performances of the sulfur cathode with the scaffolds of CNTs, carbon nanocage, and CNT/carbon nanocage composite were compared in Fig. 6c with similar sulfur loading amount and areal density. When CNTs were applied in the sulfur cathode, CNTs provided well-constructed 3D architectures with both a long-range conductive pathway for rapid electron transportation and abundant macropores with little mesoporous confined space for sulfur accommodation. Therefore, high capacity retention with a relatively low specific discharge capacity was available with an initial discharge capacity of 690 mAh g^{-1} at 0.84 A g^{-1} and a capacity retention of 69% at the current density of 8.35 A g^{-1}. In comparison, carbon nanocages provided adequate mesopores to accommodate

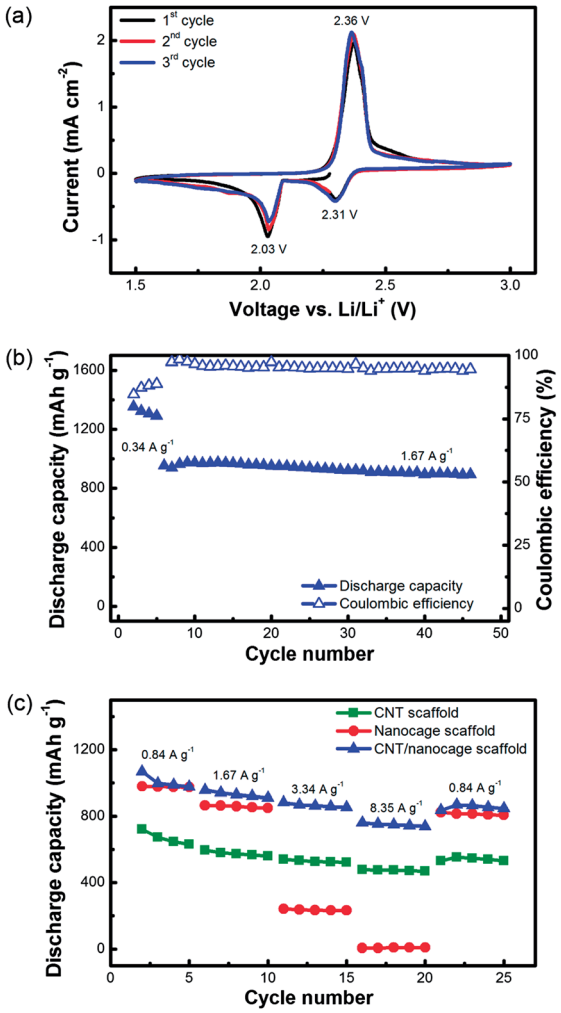

Fig. 6 (a) CV curve of the flexible sulfur electrode on CNT/carbon nanocage scaffold; (b) galvanostatic cycling performance of the flexible sulfur electrode at a charge/discharge current density of 0.34 and 1.67 A g^{-1}; (c) rate performance of sulfur electrode based on pure CNT scaffold, carbon nanocage scaffold, and CNT/carbon nanocage hybrid scaffold.

sulfur. The combination of porous carbon (*e.g.* mesoporous carbon,[22,23,32] microporous carbon[24,33]) with sp^2 nanocarbon (*e.g.* CNTs,[22,23,33] graphene,[32] and their hybrids[24]) is an efficient and effective route to improve the whole electrode for the high utilization of sulfur. Herein, carbon nanocages, instead of porous carbon, had a high pore volume, large graphene domain, excellent electrical conductivity, as well as the confined space to guarantee good stability even with a high loading amount of sulfur. However, when the carbon nanocages were simply mixed with short CNT conductive additives, the as-obtained scaffold showed a high discharge capacity only at low charge/discharge current densities, which suffered from a severe capacity drop at high current density. The discharge capacity was 978 mAh g^{-1} at 0.84 A g^{-1} in the first cycle, with a retention of 25 and 1% at 3.34 and 8.35 A g^{-1}, respectively, suggesting the poor ability of the carbon nanocages to form an interlinked conducting network within the whole electrode. The CNT/carbon nanocage hybrid scaffolds delivered an exceptional rate performance due to the rational combination of the conducting networks and sulfur accommodation building blocks into multifunctional electrode architectures. A high discharge capacity of over 1000 mAh g^{-1} can be achieved at a rate of 0.84 A g^{-1}. Even at a current density of 8.35 A g^{-1}, a reversible capacity of 750 mAh g^{-1} can still be preserved, which is 70% of that at 0.84 A g^{-1}. When compared with a CNT/sulfur cathode and carbon nanocage/sulfur cathode, a remarkable improvement in the high-rate lithium ion storage capability was achieved. Moreover, unlike commercial electrodes that need polymer binders and metal foil current collectors, this all-carbon flexible electrode can stand on its own and is free of binder or metal current collector. As the binder and metal foil current collector add redundant weight to the electrode (over 15 wt% for the cathode), they ultimately reduce the specific capacity of the electrode.[34] The swelling of polymer binders and detachment of active materials from the metal current collector also induce significant degradation of batteries. By construction of the 3D conducting network, this all-carbon flexible cathode serves as a current collector itself and avoids the problem of polymer swelling and material detachment, which is beneficial for its structural stability and electrochemical performance. This flexible cathode may combine with other flexible anode materials for the combination of flexible batteries. Flexible anode electrodes with metal oxides,[35] silicon,[36] and graphitic materials[34,37] are suitable candidates, and a pre-lithiation process is needed. If the construction of reliable flexible metal lithium anodes is well addressed, the energy density of the flexible lithium–sulfur batteries may be greatly improved.

With the rational design of a flexible electrode based on nanocarbon building blocks, a high-performance sulfur electrode was fabricated with both robust mechanical and outstanding electrochemical properties. By introducing *in situ* CVD growth, the long-range conducting ultra-long CNTs and the short-term conducting carbon nanocages as sulfur accommodation units welded together and formed a highly efficient all-carbon scaffold to fulfil the hierarchical demands in charge transfer and mechanical frameworks.

3. Conclusions

The rational design of flexible sulfur cathodes free of binder and metal current collectors based on interlinked all-carbon nanoarchitectures was demonstrated. Ultra-long CNTs were employed to form highly efficient conductive networks and MgO-templated carbon nanocages served as sulfur accommodation blocks. The carbon nanocages were generated directly and welded in the CNT networks to ensure the highly-efficient electron transfer throughout the whole electrode. Electrochemical evaluation indicated that the rationally-designed structure endowed the sulfur cathode with a high specific capacity and rate performance. The initial discharge capacity of the electrode reached up to 1354 mAh g^{-1} at 0.34 A g^{-1}. Even at a current density of 8.35 A g^{-1}, a reversible capacity of 750 mAh g^{-1} can be preserved, which was 70% of that at 0.84 A g^{-1}. This versatile method for the construction of a

flexible electrode scaffold may also find applications in other high-performance electrochemical systems, such as lithium ion batteries, supercapacitors, lithium air batteries, *etc*.

4. Experimental

Fabrication of CNT and carbon nanocage building blocks

The all-carbon flexible film was fabricated by *in situ* CVD growth on the CNT/MgO composite to ensure the interconnected nanostructures. The CNTs were synthesized through a floating catalyst CVD.[38] CNTs were then directly used to form a suspension by gaseous/liquid shearing. The porous MgO flakes were synthesized by the hydrothermal process of MgO and poly(ethylene glycol) at 200 °C, followed by filtration and high-temperature annealing at 500 °C for 3 h. The porous MgO flakes and ultra-long CNTs were dispersed in *N*-methyl pyrrolidone solvent under vigorous liquid-phase shearing. Afterwards, the co-dispersed solution was filtered through a nylon membrane (0.45 μm pore size) to collect the CNT/MgO film. After drying, the as-obtained film was used as a template for methane CVD at 950 °C to obtain the CNT/MgO@C composite. The CNT/carbon nanocage interconnected film was fabricated after removal of the MgO template by soaking in 1.0 M HCl at a moderate temperature of 60 °C.

Fabrication of flexible CNT/nanocage/sulfur cathode

The electrochemically-active material of sulfur was impregnated into the CNT/carbon nanocage scaffold through a facile liquid sulfur infiltration. The CNT/graphene scaffold films were set on a hot plate at 70 °C, and the solvent of sulfur in toluene was added onto the film dropwise to reach the expected sulfur content. Then the sulfur-containing films were heated to 155 °C under Ar atmosphere to ensure the uniform impregnation of sulfur. After being punched into disks with a diameter of 13 mm, the flexible sulfur cathode was available for electrochemical testing.

Characterizations

The morphology of the samples was characterized using a JEM 2010 (JEOL Ltd, Tokyo, Japan) TEM operated at 120.0 kV and a JSM 7401F (JEOL Ltd, Tokyo, Japan) SEM operated at 3.0 kV. The Raman spectra of the nanocarbon based samples were recorded with He–Ne laser excitation at 633 nm using a Horiba Jobin Yvon LabRAM HR800 Raman Spectrometer. The sorption isotherms were measured by N_2 adsorption/desorption using an Autosorb-IQ2-MP-C system. The specific surface areas were determined by the Brunauer–Emmett–Teller method. The pore size distribution and pore volume of the nanocarbon samples were calculated by the quenched solid state functional theory method. TGA was carried out on the samples using a TGA/DSC1 STARe system under O_2 and/or N_2 atmosphere, respectively. The resistance measurements of the samples were performed using the KDY-1 four-probe technique.

Electrochemical evaluation

Two-electrode cells using standard 2025 coil-type cells were constructed to evaluate the electrochemical performance of the all-carbon flexible cathode material for lithium–sulfur batteries. A mixed solution of 1,3-dioxlane–dimethyl ether (v/v = 1 : 1) with 1.0 mol L^{-1} lithium bis(trifluoromethanesulfonyl)imide solution was used for electrochemical evaluation. Lithium metal foil was used as the anode and the polypropylene membranes from Celgard Inc. were used as the separators. The electrolyte used for the assembly of the cell was adjusted with the amount of sulfur at 20 μL per mg of sulfur. The areal density of the lithium disk used as the anode is 30 mg cm^{-2}. The coin cells were tested in galvanostatic mode at various currents within a voltage range of 1.5–3.0 V using a Neware multichannel battery cycler. The CV measurements were performed on a Solartron 1470E electrochemical workstation at a scan rate of 0.1 mV s^{-1}. The capacities were calculated based on the mass of sulfur.

Acknowledgements

This work was supported by the National Basic Research Program of China (973 Program, 2011CB932602), China Postdoctoral Science Foundation (2012M520293, 2013T60125), and National Natural Science Foundation of China (21306103), and Research Fund for the Doctoral Program of Higher Education of China (20120002120047).

Notes and references

1 G. M. Zhou, F. Li and H. M. Cheng, *Energy Environ. Sci.*, 2014, DOI: 10.1039/c3ee43182g, and refs cited therein; H. Gwon, J. Hong, H. Kim, D.-H. Seo, S. Jeon and K. Kang, *Energy Environ. Sci.*, 2014, **7**, 538–551, and refs cited therein.

2 F. Zhang, C. Z. Yuan, J. J. Zhu, J. Wang, X. G. Zhang and X. W. Lou, *Adv. Funct. Mater.*, 2013, **23**, 3909; B. Liu, D. S. Tan, X. F. Wang, D. Chen and G. Z. Shen, *Small*, 2013, **9**, 1998.

3 X. L. Jia, Z. Chen, A. Suwarnasarn, L. Rice, X. L. Wang, H. Sohn, Q. Zhang, B. M. Wu, F. Wei and Y. F. Lu, *Energy Environ. Sci.*, 2012, **5**, 6845.

4 J.-W. Liu, W.-R. Huang, M. Gong, M. Zhang, J.-L. Wang, J. Zheng and S.-H. Yu, *Adv. Mater.*, 2013, **25**, 5910.

5 J. A. Rogers, T. Someya and Y. Huang, *Science*, 2010, **327**, 1603.

6 P. G. Bruce, S. A. Freunberger, L. J. Hardwick and J. M. Tarascon, *Nat. Mater.*, 2012, **11**, 19; Y. X. Yin, S. Xin, Y. G. Guo and L. J. Wan, *Angew. Chem., Int. Ed.*, 2013, **52**, 13186; S. S. Zhang, *J. Power Sources*, 2013, **231**, 153; M. K. Song, E. J. Cairns and Y. G. Zhang, *Nanoscale*, 2013, **5**, 2186.

7 Y. Yang, G. Zheng and Y. Cui, *Chem. Soc. Rev.*, 2013, **42**, 3018; D. W. Wang, Q. C. Zeng, G. M. Zhou, L. C. Yin, F. Li, H. M. Cheng, I. R. Gentle and G. Q. M. Lu, *J. Mater. Chem. A*, 2013, **1**, 9382.

8 X. Ji, K. T. Lee and L. F. Nazar, *Nat. Mater.*, 2009, **8**, 500; W. Weng, V. G. Pol and K. Amine, *Adv. Mater.*, 2013, **25**, 1608; L. Yu, N. Brun, K. Sakaushi, J. Eckert and M. M. Titirici, *Carbon*, 2013, **61**, 245.

9 F. G. Sun, J. T. Wang, H. C. Chen, W. C. Li, W. M. Qiao, D. H. Long and L. C. Ling, *ACS Appl. Mater. Interfaces*, 2013, **5**, 5630.
10 R. Elazari, G. Salitra, A. Garsuch, A. Panchenko and D. Aurbach, *Adv. Mater.*, 2011, **23**, 5641.
11 G. M. Zhou, D. W. Wang, F. Li, P. X. Hou, L. C. Yin, C. Liu, G. Q. Lu, I. R. Gentle and H. M. Cheng, *Energy Environ. Sci.*, 2012, **5**, 8901.
12 M. Hagen, S. Dorfler, P. Fanz, T. Berger, R. Speck, J. Tubke, H. Althues, M. J. Hoffmann, C. Scherr and S. Kaskel, *J. Power Sources*, 2013, **224**, 260; X. B. Cheng, J. Q. Huang, Q. Zhang, H. J. Peng, M. Q. Zhao and F. Wei, *Nano Energy*, 2014, **4**, 65; X. F. Liu, Q. Zhang, J. Q. Huang, S. M. Zhang, H. J. Peng and F. Wei, *J. Energy Chem.*, 2013, **22**, 341.
13 L. Wang, Z. Dong, D. Wang, F. Zhang and J. Jin, *Nano Lett.*, 2013, **13**, 6244.
14 C. F. Zhang, H. B. Wu, C. Z. Yuan, Z. P. Guo and X. W. Lou, *Angew. Chem., Int. Ed.*, 2012, **51**, 9592; N. Jayaprakash, J. Shen, S. S. Moganty, A. Corona and L. A. Archer, *Angew. Chem., Int. Ed.*, 2011, **50**, 5904.
15 J. T. Lee, Y. Zhao, S. Thieme, H. Kim, M. Oschatz, L. Borchardt, A. Magasinski, W. I. Cho, S. Kaskel and G. Yushin, *Adv. Mater.*, 2013, **25**, 4573.
16 J. Q. Huang, X. F. Liu, Q. Zhang, C. M. Chen, M. Q. Zhao, S. M. Zhang, W. C. Zhu, W. Z. Qian and F. Wei, *Nano Energy*, 2013, **2**, 314.
17 G. M. Zhou, L. C. Yin, D. W. Wang, L. Li, S. F. Pei, I. R. Gentle, F. Li and H. M. Cheng, *ACS Nano*, 2013, **7**, 5367.
18 S. L. Candelaria, Y. Y. Shao, W. Zhou, X. L. Li, J. Xiao, J. G. Zhang, Y. Wang, J. Liu, J. H. Li and G. Z. Cao, *Nano Energy*, 2012, **1**, 195, and refs cited therein; Q. Zhang, J. Q. Huang, W. Z. Qian, Y. Y. Zhang and F. Wei, *Small*, 2013, **9**, 1237, and refs cited therein; D. S. Su and G. Centi, *J. Energy Chem.*, 2013, **22**, 151, and refs cited therein.
19 K. K. Jin, X. F. Zhou, L. Z. Zhang, X. Xin, G. H. Wan and Z. P. Liu, *J. Phys. Chem. C*, 2013, **117**, 21112.
20 X. D. Huang, B. Sun, K. F. Li, S. Q. Chen and G. X. Wang, *J. Mater. Chem. A*, 2013, **1**, 13484.
21 M. Q. Zhao, Q. Zhang, J. Q. Huang and F. Wei, *Adv. Funct. Mater.*, 2012, **22**, 675.
22 D. L. Wang, Y. C. Yu, W. D. Zhou, H. Chen, F. J. DiSalvo, D. A. Muller and H. D. Abruña, *Phys. Chem. Chem. Phys.*, 2013, **15**, 9051.
23 T. Xu, J. X. Song, M. L. Gordin, H. Sohn, Z. X. Yu, S. R. Chen and D. H. Wang, *ACS Appl. Mater. Interfaces*, 2013, **5**, 11355.
24 H. J. Peng, J. Q. Huang, M. Q. Zhao, Q. Zhang, X. Y. Liu, W. Z. Qian and F. Wei, *Adv. Funct. Mater.*, 2014, **24**, DOI: 10.1002/adfm.201303296.
25 S. Thieme, J. Bruckner, I. Bauer, M. Oschatz, L. Borchardt, H. Althues and S. Kaskel, *J. Mater. Chem. A*, 2013, **1**, 9225.
26 M. Q. Zhao, X. F. Liu, Q. Zhang, G. L. Tian, J. Q. Huang, W. C. Zhu and F. Wei, *ACS Nano*, 2012, **6**, 10759.
27 S. W. Lee, N. Yabuuchi, B. M. Gallant, S. Chen, B. S. Kim, P. T. Hammond and Y. Shao-Horn, *Nat. Nanotechnol.*, 2010, **5**, 531.
28 G. H. Xu, C. Zheng, Q. Zhang, J. Q. Huang, M. Q. Zhao, J. Q. Nie, X. H. Wang and F. Wei, *Nano Res.*, 2011, **4**, 870.
29 X. L. Jia, Q. Zhang, M. Q. Zhao, G. H. Xu, J. Q. Huang, W. Z. Qian, Y. F. Lu and F. Wei, *J. Mater. Chem.*, 2012, **22**, 7050.
30 S. R. Zhao, C. M. Li, W. K. Wang, H. Zhang, M. Y. Gao, X. Xiong, A. B. Wang, K. G. Yuan, Y. Q. Huang and F. Wang, *J. Mater. Chem. A*, 2013, **1**, 3334; S. M. Zhang, Q. Zhang, J. Q. Huang, X. F. Liu, W. C. Zhu, M. Q. Zhao, W. Z. Qian and F. Wei, *Part. Part. Syst. Charact.*, 2013, **30**, 158.
31 W. Ahn, K. B. Kim, K. N. Jung, K. H. Shin and C. S. Jin, *J. Power Sources*, 2012, **202**, 394.
32 X. Y. Zhou, J. Xie, J. Yang, Y. L. Zou, J. J. Tang, S. C. Wang, L. L. Ma and Q. C. Liao, *J. Power Sources*, 2013, **243**, 993.
33 S. Xin, L. Gu, N. H. Zhao, Y. X. Yin, L. J. Zhou, Y. G. Guo and L. J. Wan, *J. Am. Chem. Soc.*, 2012, **134**, 18510.
34 S. Y. Chew, S. H. Ng, J. Z. Wang, P. Novak, F. Krumeich, S. L. Chou, J. Chen and H. K. Liu, *Carbon*, 2009, **47**, 2976.
35 X. L. Jia, Z. Chen, X. Cui, Y. T. Peng, X. L. Wang, G. Wang, F. Wei and Y. F. Lu, *ACS Nano*, 2012, **6**, 9911; X. D. Huang, B. Sun, S. Q. Chen and G. X. Wang, *Chem.–Asian J.*, 2014, **9**, 206.
36 S. L. Chou, Y. Zhao, J. Z. Wang, Z. X. Chen, H. K. Liu and S. X. Dou, *J. Phys. Chem. C*, 2010, **114**, 15862; L. B. Hu, H. Wu, Y. F. Gao, A. Y. Cao, H. B. Li, J. McDough, X. Xie, M. Zhou and Y. Cui, *Adv. Energy Mater.*, 2011, **1**, 523.
37 F. Liu, S. Y. Song, D. F. Xue and H. J. Zhang, *Adv. Mater.*, 2012, **24**, 1089.
38 Q. Zhang, J. Q. Huang, M. Q. Zhao, W. Z. Qian, Y. Wang and F. Wei, *Carbon*, 2008, **46**, 1152.